AIP | Applied Physics Letters

Rewritable three-dimensional holographic data storage via optical forces

Ali K. Yetisen, Yunuen Montelongo, and Haider Butt

Citation: Applied Physics Letters **109**, 061106 (2016); doi: 10.1063/1.4960710
View online: http://dx.doi.org/10.1063/1.4960710
View Table of Contents: http://scitation.aip.org/content/aip/journal/apl/109/6?ver=pdfcov
Published by the AIP Publishing

Rewritable three-dimensional holographic data storage *via* optical forces

Ali K. Yetisen,[1,2,a),b)] Yunuen Montelongo,[3,b)] and Haider Butt[4]
[1]*Harvard Medical School and Wellman Center for Photomedicine, Massachusetts General Hospital, 65 Landsdowne Street, Cambridge, Massachusetts 02139, USA*
[2]*Harvard-MIT Division of Health Sciences and Technology, Massachusetts Institute of Technology, Cambridge, Massachusetts 02139, USA*
[3]*Department of Chemistry, Imperial College London, South Kensington Campus, London SW7 2AZ, United Kingdom*
[4]*Nanotechnology Laboratory, School of Engineering Sciences, University of Birmingham, Birmingham B15 2TT, United Kingdom*

(Received 20 May 2016; accepted 29 July 2016; published online 10 August 2016)

The development of nanostructures that can be reversibly arranged and assembled into 3D patterns may enable optical tunability. However, current dynamic recording materials such as photorefractive polymers cannot be used to store information permanently while also retaining configurability. Here, we describe the synthesis and optimization of a silver nanoparticle doped poly(2-hydroxyethyl methacrylate-*co*-methacrylic acid) recording medium for reversibly recording 3D holograms. We theoretically and experimentally demonstrate organizing nanoparticles into 3D assemblies in the recording medium using optical forces produced by the gradients of standing waves. The nanoparticles in the recording medium are organized by multiple nanosecond laser pulses to produce reconfigurable slanted multilayer structures. We demonstrate the capability of producing rewritable optical elements such as multilayer Bragg diffraction gratings, 1D photonic crystals, and 3D multiplexed optical gratings. We also show that 3D virtual holograms can be reversibly recorded. This recording strategy may have applications in reconfigurable optical elements, data storage devices, and dynamic holographic displays. *Published by AIP Publishing.*
[http://dx.doi.org/10.1063/1.4960710]

Holography enables reconstruction of the images of the objects with intensity and wavefront information for application in imaging, data storage, and biosensors.[1] The storage of large amounts of digital information is a major problem for the technology industry; however, the production of a volumetric reconfigurable pattern over large numbers of writing and erasing cycles remains a challenge.[2] Optical forces can trap and manipulate dielectric and metal nanoparticles (NPs) with the so-called "optical tweezer" effect.[3] This phenomenon is enhanced when the NP has a size of the order of the electromagnetic wavelength.[4] Recently, this effect has been used to manipulate NPs with the interference patterns of laser beams.[5] This optical effect can be expanded to the holographic interference in volumetric media, which may allow the manipulation of NPs in 3D space. For example, nanosecond laser pulses were utilized to construct multilayer diffraction gratings in functionalized hydrogel films for sensing applications.[6] The radiation pressure occurs due to the transfer of momentum from the scattering of incident photons. Generally, the force exerted to the NP has two components: the scattering force and the gradient force.[7] In the case of two counter propagating beams, the scattering force vanishes and only the gradient force takes place. The gradient force originates from the anisotropic scattering of photons and it has a well-defined direction. Depending on the properties of the NP and the surrounding medium, the radiation pressure can be positive or negative.[8] A gradient force in the negative regime moves NPs toward regions of minimum intensity (nodes) in the standing wave.

A monomer solution consisting of hydroxyethyl methacrylate (HEMA), crosslinker ethylene dimethacrylate (EDMA), and methacrylic acid (MAA) was prepared. A $\sim 10\,\mu$m thick poly(2-hydroxyethyl methacrylate-*co*-methacrylic acid) (p(HEMA-*co*-MAA)) film was coated over a silanized glass slide by free-radical polymerization. Silver nitrate ($AgNO_3$) solution was used as the ion source to create NPs (Fig. 1(a)). This solution was diffused into the polymer matrix and lithium bromide (LiBr) was used to convert the Ag^+ ions to silver bromide (AgBr) nanocrystals (NCs) (Fig. 1(b)). This step is required to control the NP size distribution in the p(HEMA-*co*-MAA) matrix. AgBr NCs are light-sensitive; hence, they were exposed to broadband light to decrease their sensitivity to light (Fig. 1(c)). A photographic developer (JD-4) was used to reduce the AgBr NCs to silver metal (Ag^0) NPs (~50 –100 nm) in the p(HEMA-*co*-MAA) matrix (Fig. 1(d)). The developer's action was stopped by decreasing pH of the system below 3.0 (Fig. 1(e)). The unreacted AgBr NCs were extracted from p(HEMA-*co*-MAA) matrix by thiosulfate treatment (Fig. 1(f)). The resulting matrix was immediately ready to be used as the recording medium (Fig. 1(g)). Figure 1(h) shows a scanning electron microscope image (SEM) of the p(HEMA-*co*-MAA) matrix cross section having Ag^0 NPs ranging from 50 to 100 nm.

As the thickness of matrix was increased from 1 μm to 10 μm, the transmitted light intensity ($\lambda = 532$ nm) through the recording medium decreased from 64% to 46% (Fig. 1(i)). The concentration of the EDMA was also important in

a)Author to whom correspondence should be addressed. Electronic mail: ayetisen@mgh.harvard.edu
b)A. K. Yetisen and Y. Montelongo contributed equally to this work.

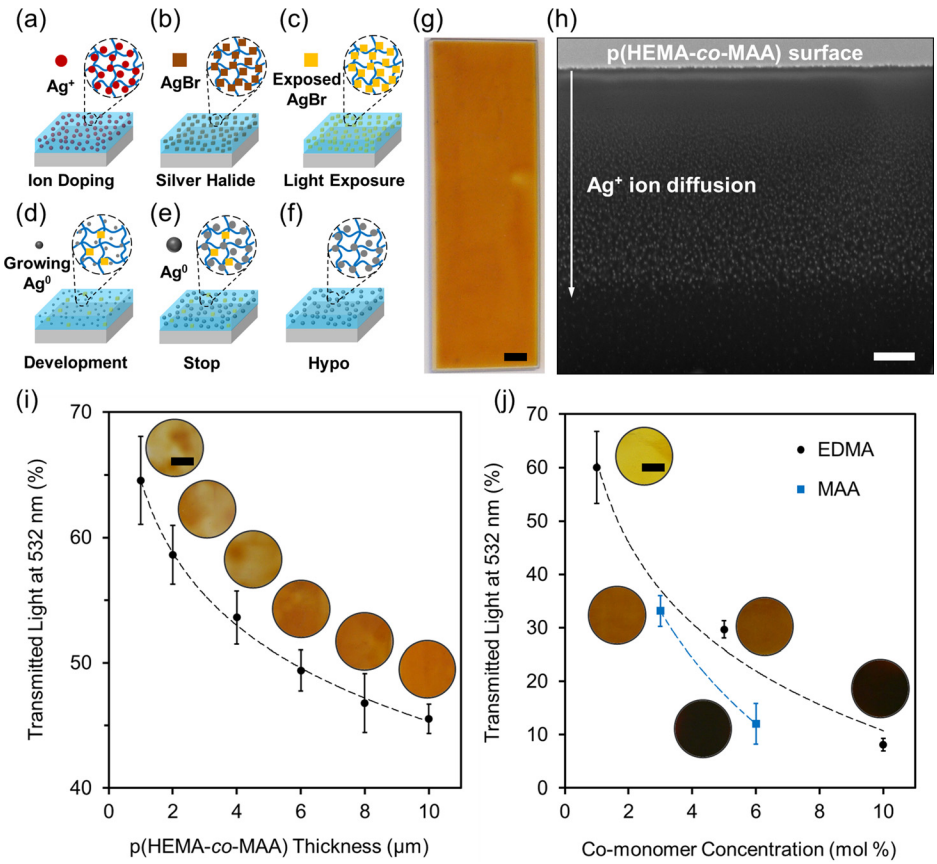

FIG. 1. Fabrication of a p(HEMA-*co*-MAA) recording medium for reconfigurable holography. (a)–(f) Formation of NPs in the medium. (g) Fabricated recording medium ($t = \sim 10\,\mu m$). Scale bar = 5 mm. (h) SEM image of the recording medium cross-section. Scale bar = 1 μm. (i) The effect of variation in thickness on light transmission through the recording medium. (j) EDMA and MAA concentrations on light transmission through the medium and Ag^0 NP density. Scale bar = 5 mm.

retaining Ag^0 NPs within the recording medium. When the concentration of EDMA was increased from 1 to 10 mol. %, the transmitted light intensity through the p(HEMA-*co*-MAA) matrix decreased from 60% to 9%, corresponding to Ag^0 NP density (1.3 vol. %) decrease of 28 vol. % (Fig. 1(j)). As the concentration of MAA was increased from 3 to 6 mol. %, the transmitted light intensity through the matrix decreased from 33% to 12%, corresponding to Ag^0 NP density increase of 25 vol. % (Fig. 1(j)). The optimized recording medium had 2.5 mol. % EDMA and 6 mol. % MAA to achieve ~50% light transmission and retain 1 vol. % Ag^0 NPs. Supplementary material provides a protocol for the fabrication of the recording medium.[9]

A Nd:YAG laser (5 ns, 532 nm, 350 mJ) was set to function in Denisyuk reflection mode.[10] The laser beam reflected from dielectric mirrors was expanded (~1 cm) and directed to the p(HEMA-*co*-MAA) matrix (Fig. 2(a)). This sample was tilted with angle θ from the surface plane of a plane mirror. The reference beam propagated through the matrix and reflected back from the mirror (Fig. 2(b)). The object beam interfered with the reference beam. This process created high intensity (antinodes) and low intensity (nodes) regions within the matrix to organize Ag^0 NPs. The combination of the reference pulse and the object pulse forms a multilayer field that allows for recording the hologram. Photoinduced ablation of NPs took place during the first recording step. The first laser exposure of light attenuated the Ag^0 NPs from 50–100 nm to 10–30 nm as the laser light was absorbed by the Ag^0 NPs. However, no ablation took place below this Ag^0 NP diameter threshold.

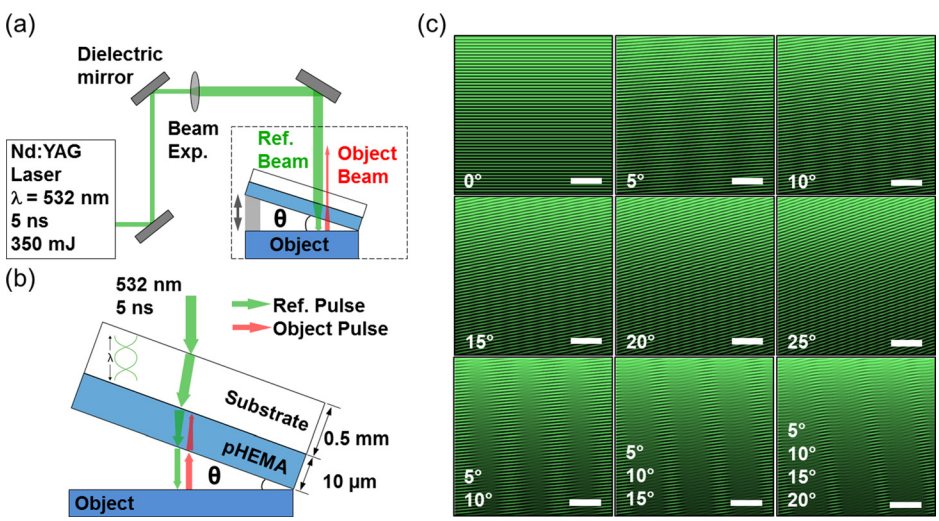

FIG. 2. Fabrication of the multilayer gratings. (a) Laser setup in Denisyuk reflection mode. (b) Formation of an interference pattern within p(HEMA-*co*-MAA) matrix. (c) Interference pattern fields at different tilt angles. Scale bars = 1 μm.

The respective intensities and phases of individual plane waves were calculated. Figure 2(c) shows normalized field intensity patterns of a medium (50% transmission) at tilt angles (θ) ranging from 0° to 25°, where the reference beam is propagated from the top. The green regions in Fig. 2(c) show the constructive interference regions while the black regions represent destructive interference. The periodicity of the standing wave was approximately half of the laser light wavelength (~266 nm), and the intensity of this multilayer pattern decreased as the tilt angle increased from 0° to 25°. Additionally, the superpositioning of waves at different tilt angles (5°–20°) showed unique patterns in which the properties of multiple waves coincided.

Finite element simulations were performed to analyze the optical properties of the multilayer gratings. COMSOL Multiphysics was used to simulate the light diffraction from the photonic structures.[11] The geometry mesh had 2 nm resolution, where the computation was performed *via* a parametric sweep. Simulated nanostructures consisted of periodic multilayers of Ag NPs within a matrix. A MATLAB code was utilized to generate normal random distribution of Ag^0 NPs (10–30 nm, $\sigma = 10$ nm) within the stacks, where the mean positions of the layers were set to lattice constants. The diffraction simulation parameters were extracted from the interference patterns modeled in Fig. 2(c), where the lattice constant was ~175 nm and the effective refractive index of the medium was 1.43. The refractive index of the domains containing Ag^0 NPs was set to the electrical conductivity of silver (61.6 mS m^{-1}). Each stack contained ~60 Ag^0 NPs within 20 layers.

To simulate the grating formation in the recording medium, randomly distributed Ag^0 NPs were modeled over $2 \times 2\ \mu m^2$ using a MATLAB code. The displacement of NPs in each pulse was proportional to their location in the wave: $\Delta \mathbf{x} \propto \sin(\mathbf{K}\ \mathbf{x})$, where $\mathbf{x}$ was the NP position and $\mathbf{K}$ was the wave vector. The constant of proportionality was inferred experimentally. In each simulation, the direction of $\mathbf{K}$ was changed to simulate the exposure angle. The refractive index of the matrix was defined as 1.37 (from the refractometer measurements). The imaginary part of the refractive index was estimated by measuring the absorption of the recording medium. A light decay of 80% was measured after passing through a thickness of 10 μm with a 532 nm laser. The imaginary part of the refractive index was 0.4542 *i*. The mean radii of the nanoparticles were set within the range of 10–30 nm. The number of Ag^0 NPs was 18 per each stack with 11 stacks in total. The exposure wavelength was defined as 532 nm and the multilayer exposure field was simulated. Figure 3(a) shows the application of simulated field to a randomized medium containing Ag^0 NPs at different angles from the surface plane of the medium to create multilayer diffraction gratings. Figure 3(b) shows the simulated optical diffraction

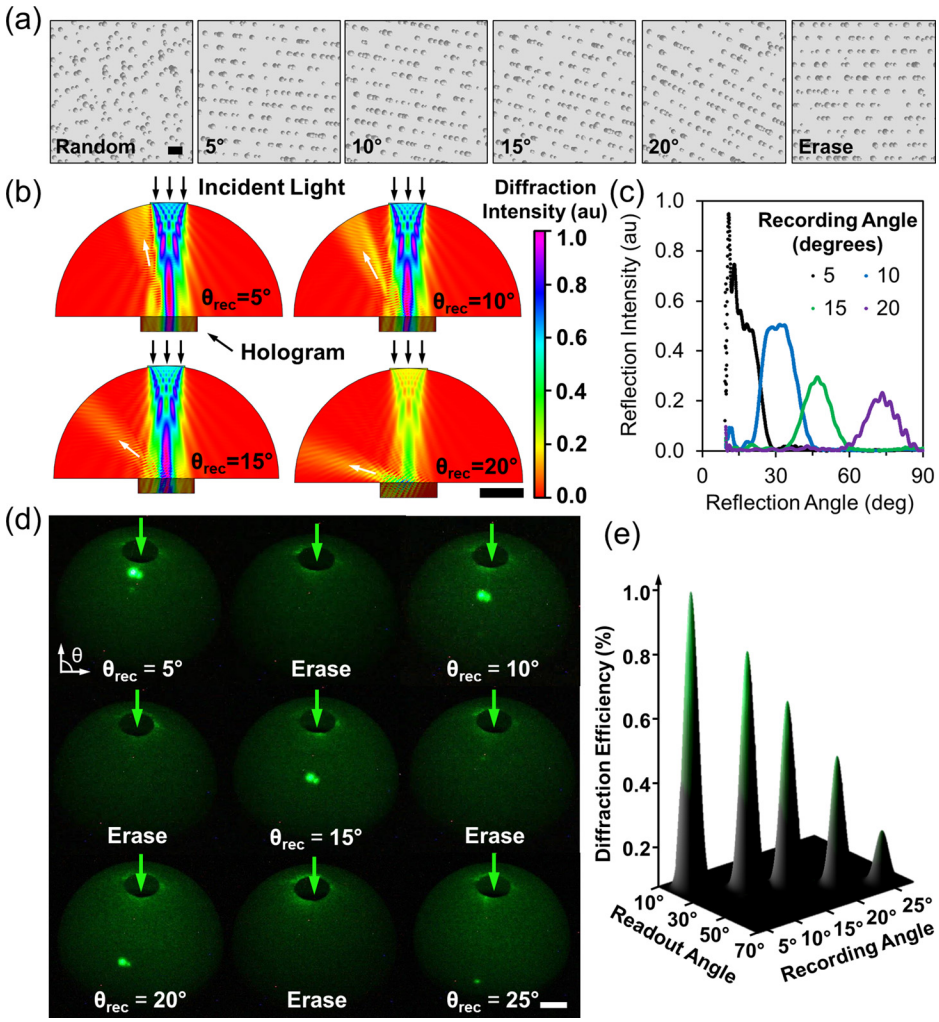

FIG. 3. Reversible holographic data storage. (a) Simulated organization of Ag^0 NPs within the recording medium at different field exposures. Scale bar = 200 nm. (b) Finite element simulations of holograms shown in a semi-transparent hemisphere. Scale bar = 20 μm. (c) Simulated optical diffraction spectra. (d) Demonstration of recording reversibility. The incident light was propagated from top. Scale bar = 1 cm. (e) Angle-resolved measurements of holograms.

through slanted holographic gratings recorded from 5° to 20° with respect to the surface plane of the matrix. To visualize the reflected light in the far field, the hologram was confined in a hemispherical computational domain. The diffraction spectra showed peak reflectivity at ~530 nm, which was consistent with the lattice spacing (~175 nm) of the grating. The holograms recorded at 5°, 10°, 15°, and 20° showed diffraction peaks at 13°, 30°, 48°, and 65°, respectively (Fig. 3(c)). The diffraction peak intensities decreased to 33%, 66%, 85% as the recording tilt angle was increased from 5° to 10°, 15°, and 20°, respectively.

To obtain the reading angle produced by a volume diffraction grating embedded in a medium with refractive index n, Bragg's law should be satisfied

$$d\ \sin(\theta'_{read}) = \lambda_{eff}, \tag{1}$$

where d is the oscillation distance of the slanted structure, θ'_{read} is the reading angle in the recording medium, and λ_{eff} is the effective wavelength (λ/n). The effective distance d is produced due to the tilt angle of the volume grating originating from the standing wave and is found with a trigonometric relation

$$2\sin(\theta_{record}) = \frac{\lambda_{eff}}{d}, \tag{2}$$

where θ_{record} is the tilt angle of the grating which is the same as the recording angle of the sample. The angle inside the recording medium is

$$\sin(\theta'_{read}) = 2\sin(\theta_{record}). \tag{3}$$

However, the reading angle (θ'_{read}) changes from the recording medium to air. Therefore, the reading angle in air θ_{read} follows Snell's law

$$n\ \sin(\theta'_{read}) = \sin(\theta_{read}). \tag{4}$$

Hence, the relation between the writing angle and the recording angle is

$$\theta_{\text{read}} = \sin^{-1}(2n\sin\theta_{\text{record}}). \tag{5}$$

To demonstrate the capability of moving NPs within the medium reversibly, the holograms were recorded at 5°, 10°, 15°, 20°, and 25° tilt angles with intermediate erasing steps (recorded at 0°). Figure 3(d) shows the first order diffracted light over a semi-transparent hemisphere as the holograms were normally illuminated with 532 nm laser light. The modulation was mostly in phase rather than in amplitude since the effective refractive index changes when NPs migrate. The measured index of refraction of the recording medium without NPs was 1.37 and with NPs was 1.43. The increase in the effective refractive index of the recording medium is due to the reduction of Ag^+ ions to Ag^0 NPs by the photographic developer. This difference in refractive index was significant enough to produce a considerable phase modulation. The change in both the real and the imaginary parts of the refractive index induces diffraction. Additionally, a periodic variation of amplitude, or phase, or both creates diffraction.[12] Furthermore, this phenomenon is observed in both transmission and reflection modes.

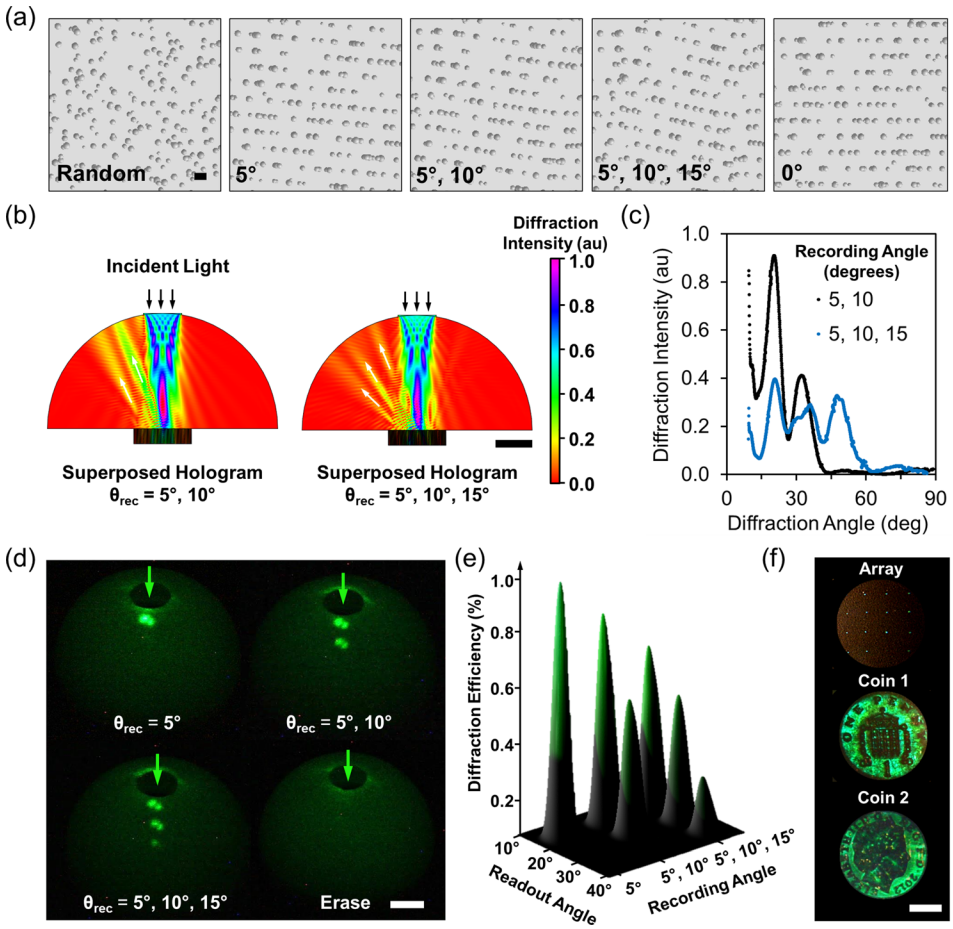

FIG. 4. Reversible recording of superposed holographic data. (a) Simulated organization of Ag^0 NPs. Scale bar = 200 nm. (b) Finite element simulations. θ_{rec} = recording tilt angle. Scale bar = 20 μm. (c) Simulated diffraction spectra. (d) Demonstration of superposed gratings on subsequent recording steps. Scale bar = 1 cm. (e) Angle-resolved measurements. (f) Rewritable holographic array and 3D virtual images of coins. Scale bar = 5 mm.

The process of hologram recording was fully reversible, demonstrated by erasing the hologram at 0° tilt angle from the surface plane of the mirror to align the first order diffracted light with specular reflection. In this holographic erasure process, the laser pulse is incident to the surface plane of the recording medium. Hence, the formed Ag NPs are organized in a multilayer structure that runs parallel to the substrate. The distance that nanoparticles move within the recording medium depends on the number and energy of the laser pulses. We recorded and erased these structures over 30–40 cycles. As the recording angle was increased, the first order diffracted light from the normal shifted from 15° to 66° (Fig. 3(e)). The decrease in the diffraction intensity with increasing diffraction angle can be attributed to the interference of the transmission grating.

Figure 4(a) illustrates simulated geometry of superimposed holographic gratings. Figure 4(b) shows simulated optical diffraction of superposed holograms recorded at 5°, 10°, and 5°, 10°, 15° with respect to the surface plane of the matrix. The holograms superposed at 5° and 10° had simulated diffraction peaks at 21° and 33°, respectively (Fig. 4(c)). When three holograms were superposed at 5°, 10°, and 15°, the diffraction peaks were at 22°, 38°, and 50° (Fig. 4(c)). The average intensity of the simulated diffraction peaks of these three diffraction spots was ~60% lower than those of the holograms superposed at 5° and 10°.

To superpose the holograms, the first hologram was recorded at 5° from the surface plane of the mirror, and subsequently the second and third holograms were recorded at 10° and 15° within the same p(HEMA-*co*-MAA) matrix. In this procedure, the hologram was not erased between the recording steps. This process allowed for superposing holographic gratings at 5°, 10°, and 15° tilt angles iteratively (Fig. 4(d)). The superposed hologram diffracted light at distinct angles. Similarly, angle-resolved measurements of the superposed holograms at 5°, 10°, and 15° tilt angles showed diffraction at 15°, 25°, and 40°, respectively (Fig. 4(e)). The intensity of the diffracted spot at 40° was lower than the spots at 15° and 25°. Figure 3(f) shows a rewritable holographic array (4 × 4) and virtual holograms of coins. During the experiments, no fatigue was observed in the p(HEMA-*co*-MAA) matrix. The recorded holograms showed full parallax and efficiently diffracted the incident light. The described simulation model and fabrication strategy to reversibly record holograms may find applications in dynamic displays, printable optical devices, and security.

The authors thank the Leverhulme Trust for research funding.

[1]M. Haw, Nature **422**(6932), 556 (2003); D. E. Smalley, Q. Y. Smithwick, V. M. Bove, Jr., J. Barabas, and S. Jolly, *ibid.* **498**(7454), 313 (2013); N. M. Farandos, A. K. Yetisen, M. J. Monteiro, C. R. Lowe, and S. H. Yun, Adv. Healthcare Mater. **4**(6), 792 (2015); A. K. Yetisen, H. Butt, and S. H. Yun, ACS Sens. **1**(5), 493 (2016); A. K. Yetisen, Y. Montelongo, M. M. Qasim, H. Butt, T. D. Wilkinson, M. J. Monteiro, and S. H. Yun, Anal. Chem. **87**(10), 5101 (2015); A. K. Yetisen, M. M. Qasim, S. Nosheen, T. D. Wilkinson, and C. R. Lowe, J. Mater. Chem. C **2**(18), 3569 (2014); A. K. Yetisen, Y. Montelongo, F. da Cruz Vasconcellos, J. L. Martinez-Hurtado, S. Neupane, H. Butt, M. M. Qasim, J. Blyth, K. Burling, J. B. Carmody, M. Evans, T. D. Wilkinson, L. T. Kubota, M. J. Monteiro, and C. R. Lowe, Nano Lett. **14**(6), 3587 (2014); A. K. Yetisen, H. Butt, F. C. Vasconcellos, Y. Montelongo, C. A. B. Davidson, J. Blyth, L. Chan, J. B. Carmody, S. Vignolini, U. Steiner, J. J. Baumberg, T. D. Wilkinson, and C. R. Lowe, Adv. Opt. Mater. **2**(3), 250 (2014); A. K. Yetisen, H. Butt, T. Mikulchyk, R. Ahmed, Y. Montelongo, M. Humar, N. Jiang, S. Martin, I. Naydenova, and S. H. Yun, "Color-selective 2.5D holograms on large-area flexible substrates for sensing and multilevel security," Adv. Opt. Mater. 2016 (published online); A. K. Yetisen, I. Naydenova, F. C. Vasconcellos, J. Blyth, and C. R. Lowe, Chem. Rev. **114**(20), 10654 (2014).
[2]L. Hesselink, S. S. Orlov, A. Liu, A. Akella, D. Lande, and R. R. Neurgaonkar, Science **282**(5391), 1089 (1998).
[3]O. M. Maragò, P. H. Jones, P. G. Gucciardi, G. Volpe, and A. C. Ferrari, Nat. Nanotechnol. **8**(11), 807 (2013).
[4]Y. Montelongo, A. K. Yetisen, H. Butt, and S. H. Yun, Nat. Commun. **7**, 12002 (2016).
[5]A. K. Yetisen, Y. Montelongo, N. M. Farandos, I. Naydenova, C. R. Lowe, and S. H. Yun, Appl. Phys. Lett. **105**(26), 261106 (2014).
[6]M. Zawadzka, T. Mikulchyk, D. Cody, S. Martin, A. K. Yetisen, J. L. Martinez-Hurtado, H. Butt, E. Mihaylova, H. Awala, S. Mintova, S. H. Yun, and I. Naydenova, in *Photonic Materials for Sensing, Biosensing and Display Devices*, edited by M. J. Serpe, Y. Kang, and Q. M. Zhang (Springer, Switzerland, 2016), p. 315.
[7]K. C. Neuman and S. M. Block, Rev. Sci. Instrum. **75**(9), 2787 (2004).
[8]M. Šiler, L. Chvátal, and P. Zemánek, J. Quant. Spectrosc. Radiat. Transfer **126**, 84 (2013).
[9]See supplementary material at http://dx.doi.org/10.1063/1.4960710 for materials, instruments, synthesis of p(HEMA-co-MAA) matrix, and fabrication of the recording medium.
[10]S. A. Benton and V. M. Bove, *Holographic Imaging* (John Wiley & Sons, Inc., 2007), p. 173; Q. Zhao, A. K. Yetisen, C. J. Anthony, W. R. Fowler, S. H. Yun, and H. Butt, Appl. Phys. Lett. **107**(4), 041115 (2015); F. C. Vasconcellos, A. K. Yetisen, Y. Montelongo, H. Butt, A. Grigore, C. A. B. Davidson, J. Blyth, M. J. Monteiro, T. D. Wilkinson, and C. R. Lowe, ACS Photonics **1**(6), 489 (2014); Q. Zhao, A. K. Yetisen, A. Sabouri, S. H. Yun, and H. Butt, ACS Nano **9**(9), 9062 (2015).
[11]A. Breuer-Weil, N. N. Almasoud, B. Abbasi, A. K. Yetisen, S. H. Yun, and H. Butt, Nanoscale Res. Lett. **11**(1), 157 (2016); C. P. Tsangarides, A. K. Yetisen, F. C. Vasconcellos, Y. Montelongo, M. M. Qasim, T. D. Wilkinson, C. R. Lowe, and H. Butt, RSC Adv. **4**(21), 10454 (2014).
[12]M. Born, E. Wolf, and A. B. Bhatia, *Principles of Optics: Electromagnetic Theory of Propagation, Interference and Diffraction of Light*, 7th ed. (Cambridge University Press, United Kingdom, 1999).